Cell Metabolism
Article

High-Mobility Group Box 1 Is Essential for Mitochondrial Quality Control

Daolin Tang,[1,8,*] Rui Kang,[1,8] Kristen M. Livesey,[1] Guido Kroemer,[2,3,4,5,6] Timothy R. Billiar,[1] Bennett Van Houten,[7] Herbert J. Zeh, III,[1] and Michael T. Lotze[1,*]
[1]Department of Surgery, G.27A Hillman Cancer Center, University of Pittsburgh Cancer Institute, Pittsburgh, PA 15219, USA
[2]INSERM, U848, 39 rue Calmette Desmoulins, 94805 Villejuif, France
[3]Metabolomics Platform, Institut Gustave Roussy, Pavillon de Recherche 1, 94805 Villejuif, France
[4]Centre de Recherche des Cordeliers, 15 rue de l'Ecole de Médecine, 75006 Paris, France
[5]Pôle de Biologie, Hôpital Européen Georges Pompidou, AP-HP, 20 rue Leblanc, 75015 Paris, France
[6]Faculté de Médecine, Université Paris Descartes, 15 rue de l'Ecole de Médecine, 75006 Paris, Paris, France
[7]Department of Pharmacology and Chemical Biology, G.27A Hillman Cancer Center, University of Pittsburgh Cancer Institute, Pittsburgh, PA 15219, USA
[8]These authors contributed equally to this work
*Correspondence: tangd2@upmc.edu (D.T.), lotzemt@upmc.edu (M.T.L.)
DOI 10.1016/j.cmet.2011.04.008

SUMMARY

Mitochondria are organelles centrally important for bioenergetics as well as regulation of apoptotic death in eukaryotic cells. High-mobility group box 1 (HMGB1), an evolutionarily conserved chromatin-associated protein which maintains nuclear homeostasis, is also a critical regulator of mitochondrial function and morphology. We show that heat shock protein beta-1 (HSPB1 or HSP27) is the downstream mediator of this effect. Disruption of the HSPB1 gene in embryonic fibroblasts with wild-type HMGB1 recapitulates the mitochondrial fragmentation, deficits in mitochondrial respiration, and adenosine triphosphate (ATP) synthesis observed with targeted deletion of HMGB1. Forced expression of HSPB1 reverses this phenotype in HMGB1 knockout cells. Mitochondrial effects mediated by HMGB1 regulation of HSPB1 expression serve as a defense against mitochondrial abnormality, enabling clearance and autophagy in the setting of cellular stress. Our findings reveal an essential role for HMGB1 in autophagic surveillance with important effects on mitochondrial quality control.

INTRODUCTION

Mitochondria play a primary role in bioenergetics in most eukaryotic cells (Chan, 2006a). Gene products derived from both the mitochondrial and nuclear genomes (Poyton and McEwen, 1996) are necessary for the assembly and function of respiratory-competent mitochondria. High-mobility group box 1 (HMGB1) is an evolutionarily conserved protein, found in abundance within the nucleus. HMGB1 knockout mice die shortly after birth with severe hypoglycemia, pointing to the essential nature of the protein (Calogero et al., 1999). Within the nucleus, HMGB1 binds and bends DNA, facilitating numerous nuclear functions including maintenance of genome stability, transcription, replication, recombination, and repair. HMGB1 plays a role in neurodegeneration, aging, and cancer (Kang et al., 2010b; Lotze and Tracey, 2005; Qi et al., 2007; Tang et al., 2010c, 2011), which are often accompanied by mitochondrial abnormalities (Chan, 2006b; Poyton and McEwen, 1996). It can be rapidly mobilized to other sites in the cell as well as actively released from cells. This study was initiated to determine whether HMGB1 affects mitochondrial function.

RESULTS AND DISCUSSION

To address this possibility, we first assessed real-time oxidative phosphorylation (OXPHOS) by determining the oxygen consumption rate (OCR) and glycolysis by measuring the extracellular acidification rate (ECR) with an extracellular flux analyzer (Qian and Van Houten, 2010; Wu et al., 2007) in Hmgb1$^{+/+}$ wild-type and Hmgb1$^{-/-}$ knockout immortalized mouse embryonic fibroblasts (MEFs) (Figure 1A). Analysis of OCR and ECR was performed in the presence of four individual inhibitors: (1) oligomycin (Olig), which inhibits mitochondrial adenosine triphosphate (ATP) synthesis; (2) p-trifluoromethoxy carbonyl cyanide phenyl hydrazone (FCCP), which uncouples OXPHOS; (3) 2-deoxyglucose (2DG), which inhibits hexokinase in the glycolytic pathway; and (4) rotenone (Rote), which inhibits complex I in the respiratory chain. There was a significant decrease in basal OXPHOS and glycolysis with HMGB1 deficiency (+/+ versus −/−, $p < 0.001$) (Figure 1B) as well as substantial decreases in reserve capacity (FCCP stimulated OCR). To determine whether alterations in mitochondrial function are directly due to the loss of HMGB1, we transfected a plasmid expressing HMGB1 and a downstream green fluorescent protein (GFP) cDNA (to assess transfection efficiency) into Hmgb1$^{-/-}$ MEFs. Expression of HMGB1 restored glycolysis, mitochondrial respiration, and ATP production (Figures 1A–1C). To further rule out the possibility that decreased mitochondrial respiration in the Hmgb1$^{-/-}$ MEFs resulted from chronic metabolic or other unrelated genetic changes that may have occurred during clonal

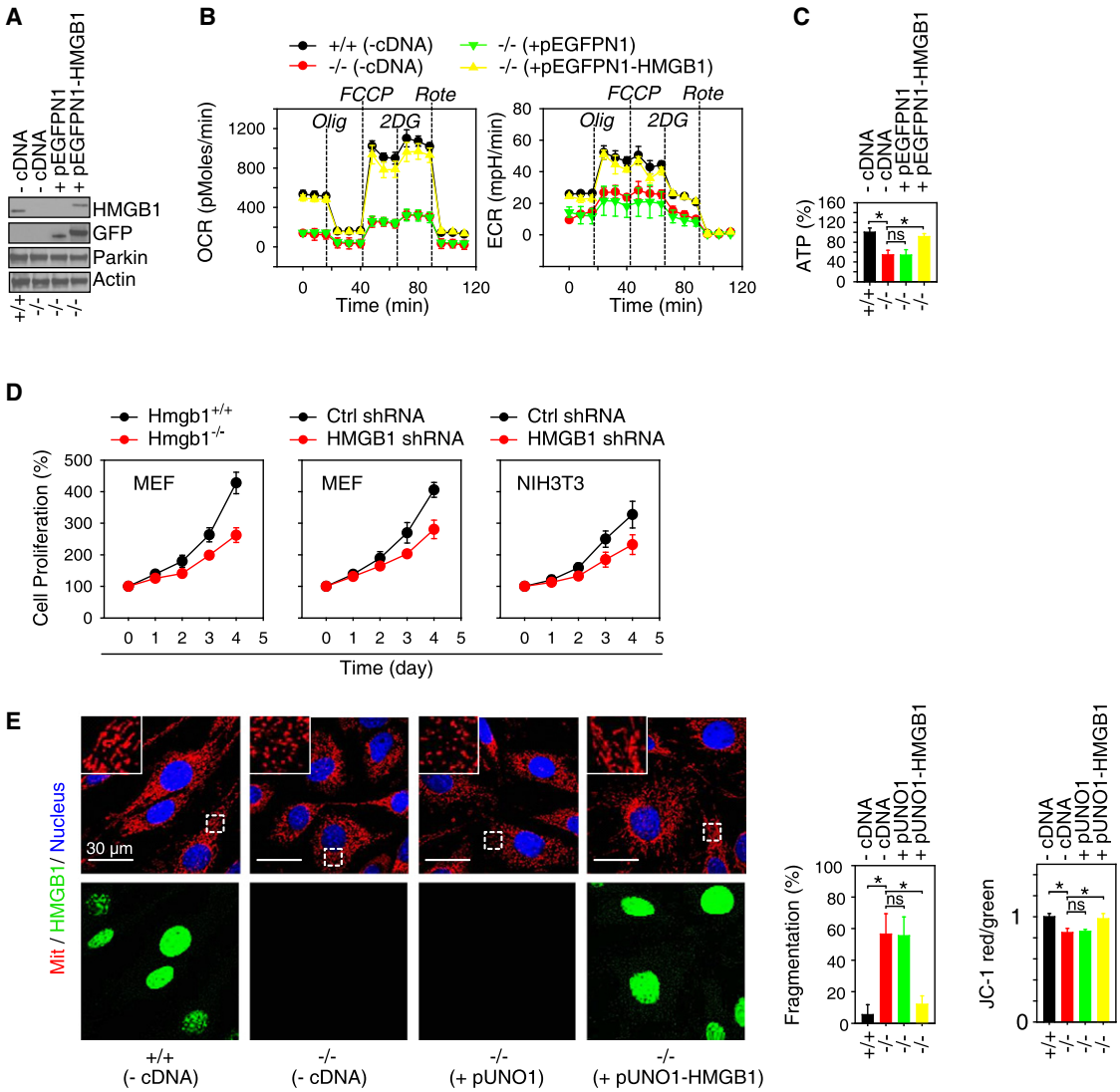

Figure 1. HMGB1 Sustains Cellular Bioenergetics and Normal Mitochondrial Morphology in MEFs

(A) Transient transfection of HMGB1 (pEGFPN1-HMGB1) or empty vector (pEGFPN1) into Hmgb1$^{-/-}$ MEFs increased HMGB1 protein expression after 48 hr by western blot assay. +/+, Hmgb1$^{+/+}$ MEFs; −/−, Hmgb1$^{-/-}$ MEFs.

(B) Expression of HMGB1 restores normal cellular bioenergetics in Hmgb1$^{-/-}$ MEFs. Cells were treated sequentially as indicated with oligomycin (Olig, 1 uM), p-trifluoromethoxy carbonyl cyanide phenyl hydrazone (FCCP, 0.3 uM), 2-deoxyglucose (2DG, 100 mM) and rotenone (Rote, 1 uM). OCR, indicative of OXPHOS, and ECR, indicative of glycolysis, were monitored by using the Seahorse Bioscience Extracellular Flux Analyzer in real time (mean ± SD, n = 3). +/+, Hmgb1$^{+/+}$ MEFs; −/−, Hmgb1$^{-/-}$ MEFs.

(C) ATP levels were assessed by using an ATP Assay Kit (PerkinElmer) in Hmgb1$^{-/-}$ (−/−) MEFs with or without pEGFPN1 empty vector or pEGFPN1-HMGB1 transfection. Data represent relative ATP levels, with Hmgb1$^{+/+}$ (+/+) MEFs set as 100% (mean ± SD, n = 3, *p < 0.01, ns, not significant).

(D) Knockout or knockdown of HMGB1 decreases cellular proliferation in MEFs and NIH 3T3 cells. Data are expressed as means ± SD.

(E) Mitochondrial (Mit) morphology was evaluated by using antibodies against mitochondrial complex I subunit GRIM-19 (red) with or without pUNO1 empty vector or pUNO1-HMGB1 transfection. HMGB1 and the nucleus were stained by HMGB1 antibody (green) or Hoechst 33342 (blue), respectively. Mitochondrial fragmentation (%) in Hmgb1$^{+/+}$ (+/+) and Hmgb1$^{-/-}$ (−/−) MEFs were quantified from 15–20 random fields. In parallel, the mitochondrial membrane potential was assayed for JC-1 expression by flow cytometry (mean ± SD, n = 3, *p < 0.01, ns, not significant, Hmgb1$^{+/+}$ group set as 1). The boxed areas represent expanded regions (magnified) from the panels of the selected region by confocal imaging.

selection, we examined OCR and ECR after reducing HMGB1 expression by short hairpin RNA (shRNA). Decreased HMGB1 expression in parental MEFs, NIH-3T3 mouse fibroblasts, Panc02 mouse, Panc2.03 human pancreatic cancer cells, or human HCT116 colon cancer cells resulted in decreased OXPHOS, phenocopying HMGB1-deficient cells (Figures 2 and 3). Furthermore, steady-state levels of ATP are decreased by 20–40% in Hmgb1$^{-/-}$ or HMGB1 knockdown cells (Figures 1C, 2C, and 3C), which is accompanied by diminished cell growth and proliferation (Figure 1D). To determine whether the deficiency in mitochondrial respiration in Hmgb1$^{-/-}$ cells is due to a decrease in mitochondrial mass, we quantified levels of representative

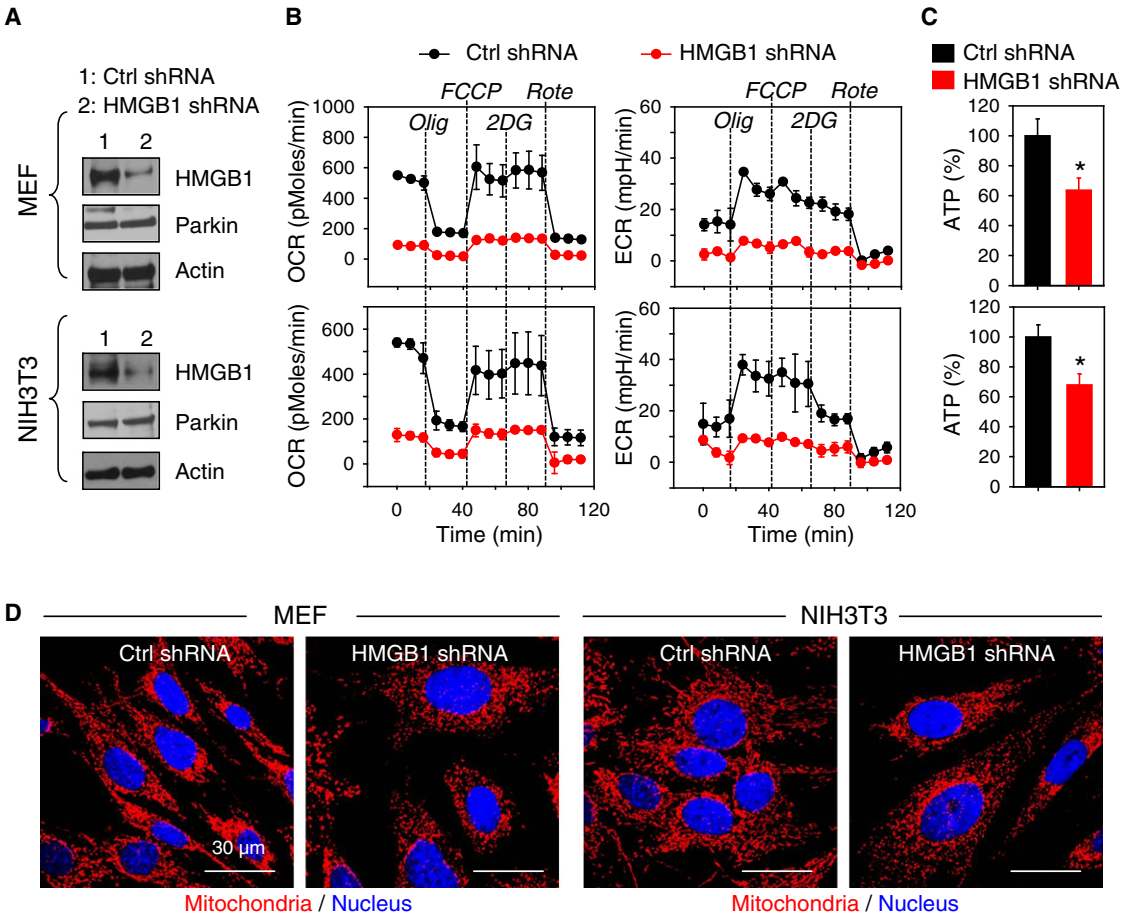

Figure 2. HMGB1 Is Required to Sustain Cellular Bioenergetics and Mitochondrial Morphology in MEFs and NIH 3T3 Cells

(A) Western blot assay for HMGB1 expression in the indicated cells after transfection for 48 hr with control shRNA or HMGB1 shRNA.

(B) Knockdown of HMGB1 in MEFs or NIH 3T3 cells decreased OXPHOS. Cells were sequentially treated as indicated with oligomycin (Olig, 1 uM), p-trifluoromethoxy carbonyl cyanide phenyl hydrazone (FCCP, 0.3 uM), 2-deoxyglucose (2DG, 100 mM), and rotenone (Rote, 1 uM). OCR, indicative of OXPHOS, and ECR, indicative of glycolysis, were monitored by using the Seahorse Bioscience Extracellular Flux Analyzer in real time (mean ± SD, n = 3).

(C) ATP levels were assessed by using an ATP Assay Kit (PerkinElmer Life Sciences) in control shRNA or HMGB1 shRNA-transfected cells. Data represent relative ATP levels, with control shRNA group set as 100% (mean ± SD, n = 3, *p < 0.01).

(D) Mitochondrial morphology was evaluated by using antibody against the mitochondrial complex I subunit GRIM-19 (red) in control shRNA or HMGB1 shRNA-transfected cells. Images are representative of 15–20 random fields. All data are representative of two or three experiments. Note in particular the fragmented mitochondria and larger nuclei in Hmgb1$^{-/-}$ cells.

proteins from complexes I–IV '(listed in Figure S1A, available online) in Hmgb1$^{+/+}$ and Hmgb1$^{-/-}$ MEFs by immunoblotting. All of the measured proteins were expressed at similar levels in both cell types. In contrast, we observed an increase in mitochondrial mass in Hmgb1$^{-/-}$ MEFs by MitoTracker Green staining (Figure S1B) or Coomassie brilliant blue staining (Figure S1C).

Mitochondria are dynamic organelles and their morphologic changes are tightly associated with their function (Chan, 2006a, 2006b). To assess the effect of HMGB1 on mitochondrial morphology, we visualized mitochondrial architecture by using immunohistochemistry with antibodies against complex I subunit GRIM-19. Morphological analysis revealed that the mitochondria, which exhibit long and tubular morphology in Hmgb1$^{+/+}$ cells, became dramatically shorter and rounder in Hmgb1$^{-/-}$ cells (Figure 1E). Moreover, expression of Hmgb1 cDNA in Hmgb1$^{-/-}$ MEFs restored mitochondrial morphology. HMGB1-deficient cells exhibit mitochondrial dysfunction with respiratory deficits, a fragmented morphology, and loss in the mitochondrial membrane potential (Figure 1E). In addition, a balance between fission and fusion is critical to maintain proper mitochondrial morphology and function. The key mediators of mitochondrial fusion and fission include dynamin-related protein 1 (DRP1), fission 1 (FIS1), optic atrophy 1 (OPA1), mitofusin 1 (MEN1), and mitofilin (Chan, 2006a, 2006b). All of these mediators are present in similar amounts in whole-cell lysate of both Hmgb1$^{+/+}$ and Hmgb1$^{-/-}$ cells (Figure S1A). However, the short and long forms (S and L) of OPA1 (Suen et al., 2008) are decreased in isolated mitochondria of Hmgb1$^{-/-}$ cells (Figure S1A).

Heat shock proteins (HSPs) and mitochondrial autophagy (mitophagy) have also been proposed to regulate mitochondrial dynamics and quality (Kim et al., 2007; Tatsuta and Langer,

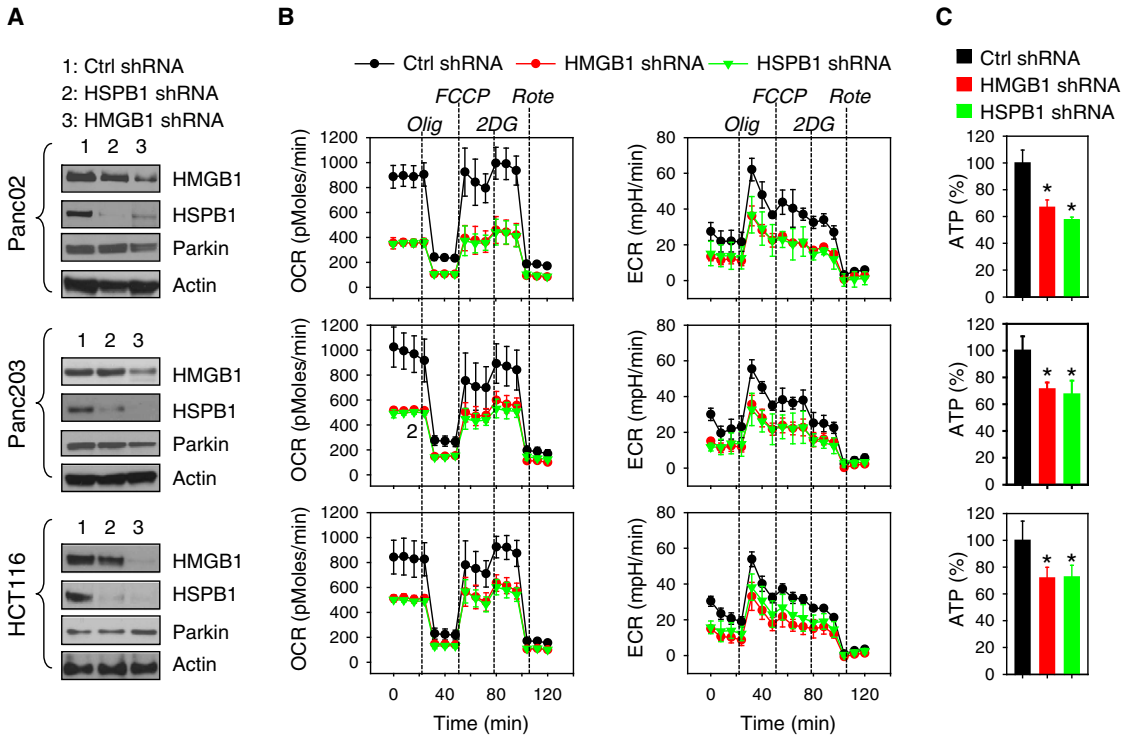

Figure 3. HMGB1 and HSPB1 Are Required to Sustain OXPHOS in Pancreatic and Colon Tumor Cells

(A) Western blot assay for HMGB1 expression in the indicated cells after transfection for 48 hr with control shRNA, HMGB1 shRNA, or HSPB1 shRNA.

(B) Knockdown of HMGB1 or HSPB1 in pancreatic and colon tumor cells decreased OXPHOS (coincident curves below control). Cells were sequentially treated as indicated with oligomycin (Olig, 1 uM), p-trifluoromethoxy carbonyl cyanide phenyl hydrazone (FCCP, 0.3 uM), 2-deoxyglucose (2DG, 100 mM), and rotenone (Rote, 1 uM). OCR, indicative of OXPHOS, and ECR, indicative of glycolysis were monitored by using the Seahorse Bioscience Extracellular Flux Analyzer in real time (mean ± SD, n = 3).

(C) ATP levels were assessed by using an ATP Assay Kit (PerkinElmer Life Sciences) in control shRNA, HMGB1 shRNA, or HSPB1 shRNA-transfected cells. Data represent relative ATP levels, with the control shRNA group set as 100% (mean ± SD, n = 3, *$p < 0.01$ versus control shRNA group). All data are representative of two or three experiments.

2008; Youle and Narendra, 2011). The principal HSPs that have chaperone activity belong to several families: HSP100 (e.g., HSP110), HSP90, HSP70, HSP60, HSP40, and the small heat-shock proteins (e.g., HSP beta-1 [HSPB1], αB-crystallin, and HSP27) (Craig et al., 1994; Sorger, 1991). In erythroid cells, NIX (also known as BNIP3L), a member of the Bcl-2 gene family, is required for mitophagy (Schweers et al., 2007). The protein expression of HSPB1 (also known as HSP25 in mice and HSP27 in humans), but not other HSPs or NIX, is significantly inhibited in Hmgb1$^{-/-}$ cells (Figure 4A). Like HMGB1 (Calogero et al., 1999), HSPB1 is expressed in various cell types and tissues, and the failure to obtain knockout mice suggests that HSPB1 is essential for growth and development (Arrigo, 2007; Garrido, 2002). Expression of HMGB1 restored HSPB1 mRNA and protein expression that were reduced in Hmgb1$^{-/-}$ cells (Figure 4B). Furthermore, we confirmed a similar HMGB1-dependent regulation of HSPB1 protein expression after heat shock, which was not observed in expression of HSP70 (Figure 4C). In both Hmgb1$^{+/+}$ and Hmgb1$^{-/-}$ cells, there are similar levels of heat shock factor 1 (HSF1), the major heat shock transcription factor that regulates stress-inducible synthesis of HSPs (Sorger, 1991), and heat shock element (HSE) activity (Figures 4A and 4D). These results reveal that HSPB1 levels are regulated by HMGB1.

To determine whether loss of HSPB1 can mimic HMGB1-deficiency, we reduced HSPB1 expression levels by about 80% by using two individual shRNA in Hmgb1$^{+/+}$ MEFs when compared with control shRNA. Decreased HSPB1 expression resulted in reduced OCR, ECR (Figures 3B and 4E), ATP production (Figures 3C and 4F), and increased mitochondrial fragmentation (Figure 4G), which was remarkably similar to the phenotype of HMGB1-deficient cells (Figure 1). To also determine whether HMGB1 regulates mitochondrial quality directly through HSPB1, we expressed mouse HSPB1 cDNA in Hmgb1$^{-/-}$ MEFs. Expression of HSPB1 in Hmgb1$^{-/-}$ cells at the physiological level observed in the Hmgb1$^{+/+}$ cells (Figure 5A) corrected the deficit in mitochondrial respiration (Figure 5B), ATP production (Figure 5C) and mitochondrial fragmentation (Figure 5D) observed in HMGB1-deficient cells. This suggests that HSPB1 expression can rescue the mitochondrial phenotype observed in HMGB1-deficient cells.

The increased number of dysfunctional mitochondria in cells deficient in HMGB1 thus appears to be due to the loss of one of HMGB1's transcriptional targets, HSPB1. Autophagy (which includes macro-, micro-, and chaperone-mediated autophagy) is an important biological mechanism for the elimination of damaged or obsolete macromolecules and organelles (Kroemer

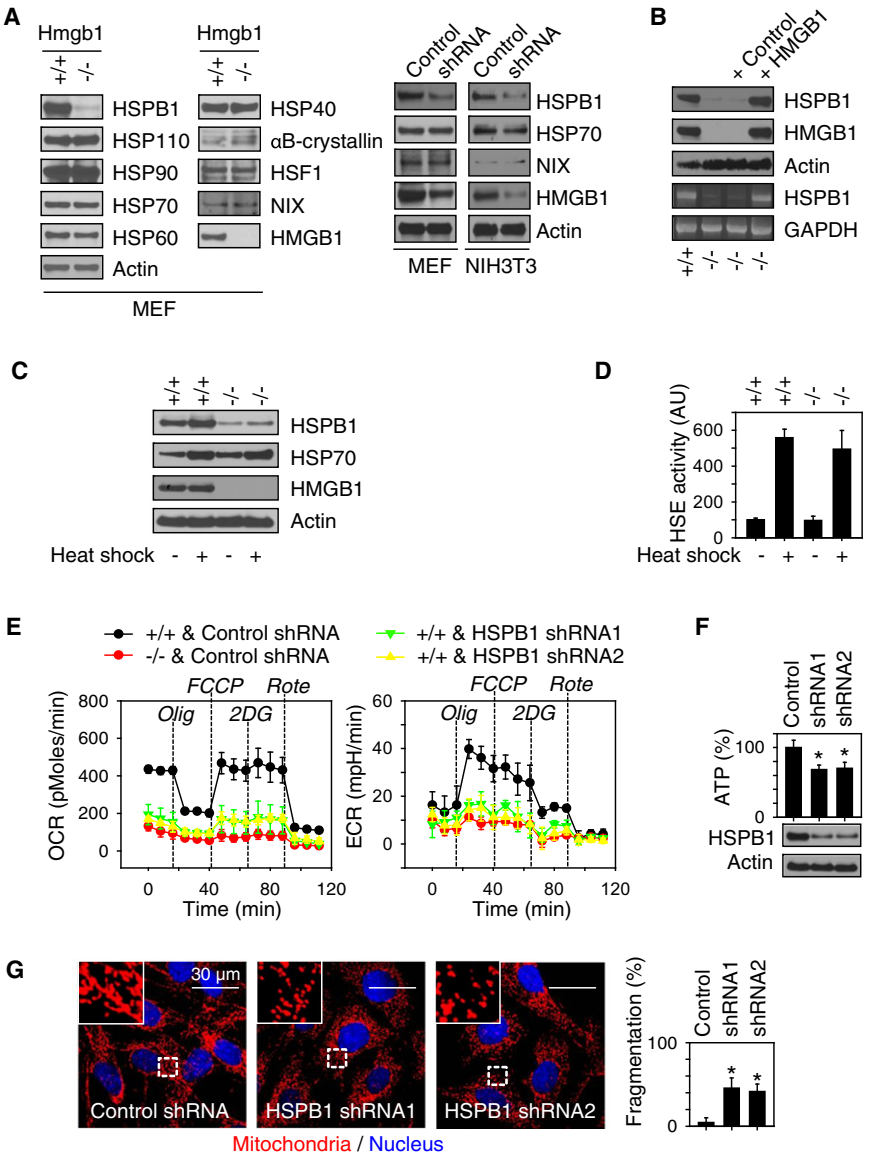

Figure 4. Knockdown of HSPB1 Recapitulates the HMGB1-Deficient Metabolic Phenotype and Mitochondrial Morphology

(A) HMGB1 regulates HSPB1 but not other HSP protein levels. Western blot analyses of HSPB1 and other proteins implicated in mitochondrial morphology in Hmgb1$^{+/+}$ (+/+) and Hmgb1$^{-/-}$ (−/−) MEFs and MEFs or NIH3T3 cells transfected with control shRNA or HMGB1 shRNA are shown.

(B) Dependence of HSPB1 protein and mRNA transactivation levels on HMGB1. Transient transfection of pUNO1-HMGB1 (HMGB1) into Hmgb1$^{-/-}$ MEFs restored HSPB1 protein expression by western blot assay (top panel) and HSPB1 mRNA expression by reverse transcription polymerase chain reaction (bottom panel). +/+, Hmgb1$^{+/+}$ MEFs; −/−, Hmgb1$^{-/-}$ MEFs.

(C) Western blot analysis of HSPB1 and HSP70 expression in Hmgb1$^{+/+}$ and Hmgb1$^{-/-}$ MEFs after heat shock (60 min in a 42.5°C water bath, then 12 hr recovery).

(D) In parallel, heat shock element (HSE) activity was evaluated in a luciferase reporter assay. Data are expressed as means ± SD (n = 3). AU, arbitrary unit.

(E) Knockdown of HSPB1 by shRNA reproduces the bioenergetic phenotype observed in HMGB1-deficient cells. The indicated cells were treated sequentially with oligomycin (Olig, 1 uM), p-trifluoromethoxy carbonyl cyanide phenyl hydrazone (FCCP, 0.3 uM), 2-deoxyglucose (2DG, 100 mM) and rotenone (Rote, 1 uM). OCR, indicative of OXPHOS, and ECR, indicative of glycolysis, were monitored by using the Seahorse Bioscience Extracellular Flux Analyzer in real time (mean ± SD, n = 3). +/+, Hmgb1$^{+/+}$ MEFs; −/−, Hmgb1$^{-/-}$ MEFs.

(F) ATP levels were assessed in MEFs transfected with HSPB1 shRNA. Data represent relative ATP levels, with control shRNA MEFs set as 100% (mean ± SD, n = 3, *p < 0.01 versus control shRNA group).

(G) Mitochondrial morphology was evaluated by using an antibody against the mitochondrial complex I subunit GRIM-19 (red). Mitochondrial fragmentation numbers (%) in cells were quantified from 15–20 random fields (mean ± SD, *p < 0.01 versus control shRNA group). All data are representative of two or three experiments. The boxed areas represent expanded regions (magnified) from the panels of the selected region by confocal imaging.

et al., 2010; Yang and Klionsky, 2010). Mitophagy is responsible for elimination of dysfunctional and impaired mitochondria (Kim et al., 2007; Youle and Narendra, 2011). Mitophagy involves at least a three-step process: (1) autophagosome formation to engulf the dysfunctional mitochondria, (2) lysosome-autophagosome fusion, and (3) degradation of dysfunctional mitochondria by autolysosomes. Blocking the formation of autophagosomes by 3-methyladenine (3-MA, class III phosphoinositide 3-kinase inhibitor) (Stroikin et al., 2004), blocking the fusion of autophagosomes with lysosomes by bafilomycin A1 (vacuolar ATPase inhibitor) (Bjørkjøy et al., 2005), or blocking lysosomal degradation by pepstatin and E64D (lysosomal protease inhibitors) (Mizushima and Yoshimori, 2007) increased rotenone-mediated ATP depletion and mitochondrial fragmentation in MEF cells (Figures S2A and S2B). In addition, autophagy inhibitors (e.g., 3-MA and bafilomycin A1) decreased OCR and ECR (Figure S2C). Our findings support the notion that autophagy and mitophagy are involved in sustaining mitochondrial respiration and morphology after cellular stress and mitochondrial injury.

Inhibition of the mitochondrial respiratory chain complex I by rotenone induces autophagy or apoptosis in a variety of cells by mediating ATP depletion, generating reactive oxygen species (ROS), or causing mitochondrial depolarization (Chen et al., 2007; Clark et al., 2006; Moon et al., 2005) (Figure 6A). We focused on the early stages of mitochondrial injury induced by rotenone because autophagy preceded mitochondria-mediated

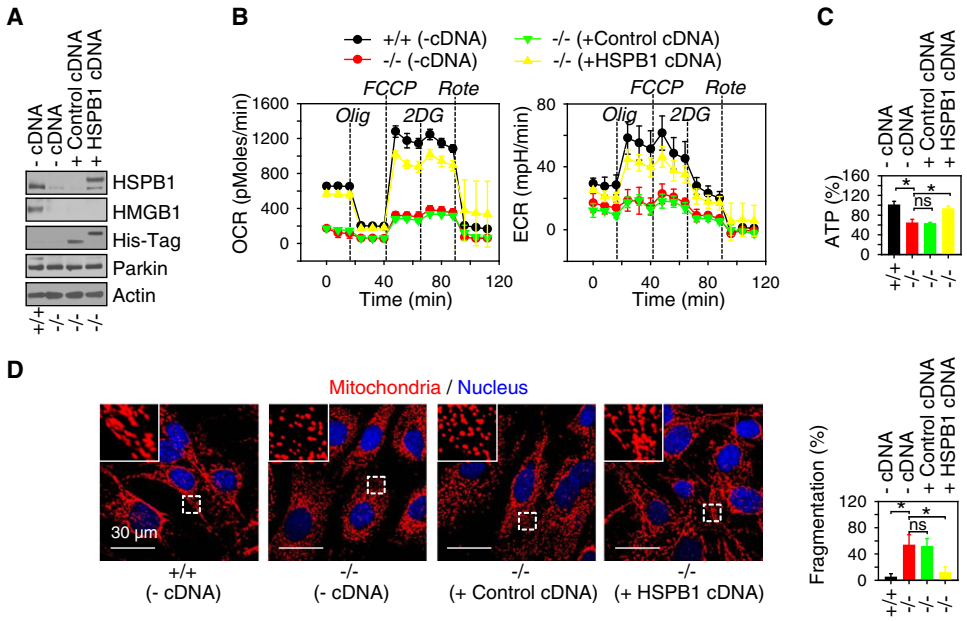

Figure 5. HSPB1 Expression Restores Cellular Bioenergetics and Mitochondrial Morphology in Hmgb1$^{-/-}$ MEFs

(A) Transient transfection of pcDNA4-HisMaxC-HSPB1 (HSPB1 cDNA) into Hmgb1$^{-/-}$ MEFs increased HSPB1 protein expression after 48 hr as determined by western blot assay. +/+, Hmgb1$^{+/+}$ MEFs; −/−, Hmgb1$^{-/-}$ MEFs; Control cDNA, pcDNA4-HisMaxC.

(B) Expression of HSPB1 rescues alterations in cellular bioenergetics in Hmgb1$^{-/-}$ MEFs. Cells were sequentially treated as indicated with oligomycin (Olig, 1 uM), p-trifluoromethoxy carbonyl cyanide phenyl hydrazone (FCCP, 0.3 uM), 2-deoxyglucose (2DG, 100 mM), and rotenone (Rote, 1 uM). OCR, indicative of OXPHOS, and ECR, indicative of glycolysis, were monitored by using the Seahorse Bioscience Extracellular Flux Analyzer in real time (mean ± SD, n = 3). +/+, Hmgb1$^{+/+}$ MEFs; −/−, Hmgb1$^{-/-}$ MEFs.

(C) ATP levels were assessed in Hmgb1$^{-/-}$ MEFs with or without HSPB1 cDNA transfection. Data represent relative ATP levels, with Hmgb1$^{+/+}$ MEFs set as 100% (mean ± SD, n = 3, *p < 0.01, ns, not significant). +/+, Hmgb1$^{+/+}$ MEFs; −/−, Hmgb1$^{-/-}$ MEFs.

(D) Mitochondrial morphology was evaluated by using an antibody against the mitochondrial complex I subunit, GRIM-19 (red). Mitochondrial fragmentation as a percent of cells was quantified in 15–20 random fields (mean ± SD, *p < 0.01, ns, not significant). +/+, Hmgb1$^{+/+}$ MEFs; −/−, Hmgb1$^{-/-}$ MEFs. All data are representative of two or three experiments. The boxed areas represent expanded regions (magnified) from the panels of the selected region by confocal imaging.

apoptosis in MEFs (Figures S2D and S2E). There was a significant increase in mitochondrial fragmentation after rotenone treatment in HMGB1- and HSPB1-deficient cells (Figures S2F and S2G). The microtubule-associated protein light chain-3 (LC3), a mammalian homolog of Atg8, is thought to recruit mitochondria into autophagosomes. Loss of HMGB1 or HSPB1 inhibited amino acid- and ATP depletion-induced autophagy as assessed by the expression of LC3-II (Figure 6C), LC3 punctae (Figures S3A and S3B), and lysosomal-associated membrane protein 2 (LAMP2) with LC3 colocalization (Figure S3D). Loss of HMGB1 and HSPB1 also decrease the mitochondrial membrane potential and increase apoptosis (Figure S3B). Moreover, autophagy inhibitors (e.g., 3-MA) increased rotenone-induced apoptosis (Figure S3C), suggesting that autophagy is a cell survival mechanism under stress. To determine whether HMGB1 and HSPB1 specifically regulate mitophagy, we assessed the process of mitophagy in the absence of HMGB1 or HSPB1. Indeed, loss of HMGB1 and HSPB1 decreased colocalization of mitochondria not only with LC3, but also with LAMP2 (Figure 6A and Figure S4), suggesting that the loss of HMGB1 or HSPB1 results in defective autophagy with secondary consequences on mitochondria.

Ultrastructural EM analysis reveals that wild-type cells exhibit normal mitochondrial morphology with fragments of mitochondria present in some autophagosomes or lysosomes after mitochondrial injury induced by rotenone (Figure 6B). As expected, polyubiquitin-binding protein, sequestosome 1 (p62) bodies and expression (Bjørkøy et al., 2005) are increased in HMGB1- and HSPB1-deficient cells when rotenone-induced autophagy is impaired (Figure 6C and Figures S5A and S5B). In addition, the degradation of exogenously introduced p62 after starvation is also impaired in HMGB1- and HSPB1-deficient cells (Figure S5C).

A well-characterized function of HSPB1 is to interact with the actin cytoskeleton (Lavoie et al., 1993a, 1993b), a dynamic structure that maintains cell shape, enables cellular locomotion and plays important roles in the transport and morphology of intracellular vesicles and organelles including mitochondria (Boldogh and Pon, 2006). Stress fibers, which are bundles of easily visualized actin filaments, appear in response to rotenone-induced mitochondrial injury. The colocalization of mitochondria and actin is also increased after rotenone treatment in wild-type cells (Figure 6A), indicating that such interactions are an important regulatory mechanism after mitochondrial injury. Similar to HMGB1 deficiency, treatment of wild-type cells with the cytoskeleton inhibitor cytochalasin D (CytD) decreases stress fibers and colocalization of mitochondria with actin, mitochondria with autophagosomes (e.g., LC3), and mitochondria with autolysosomes (e.g., LAMP2) after mitochondrial injury (Figure 6A). Moreover, CytD increases rotenone-induced apoptosis

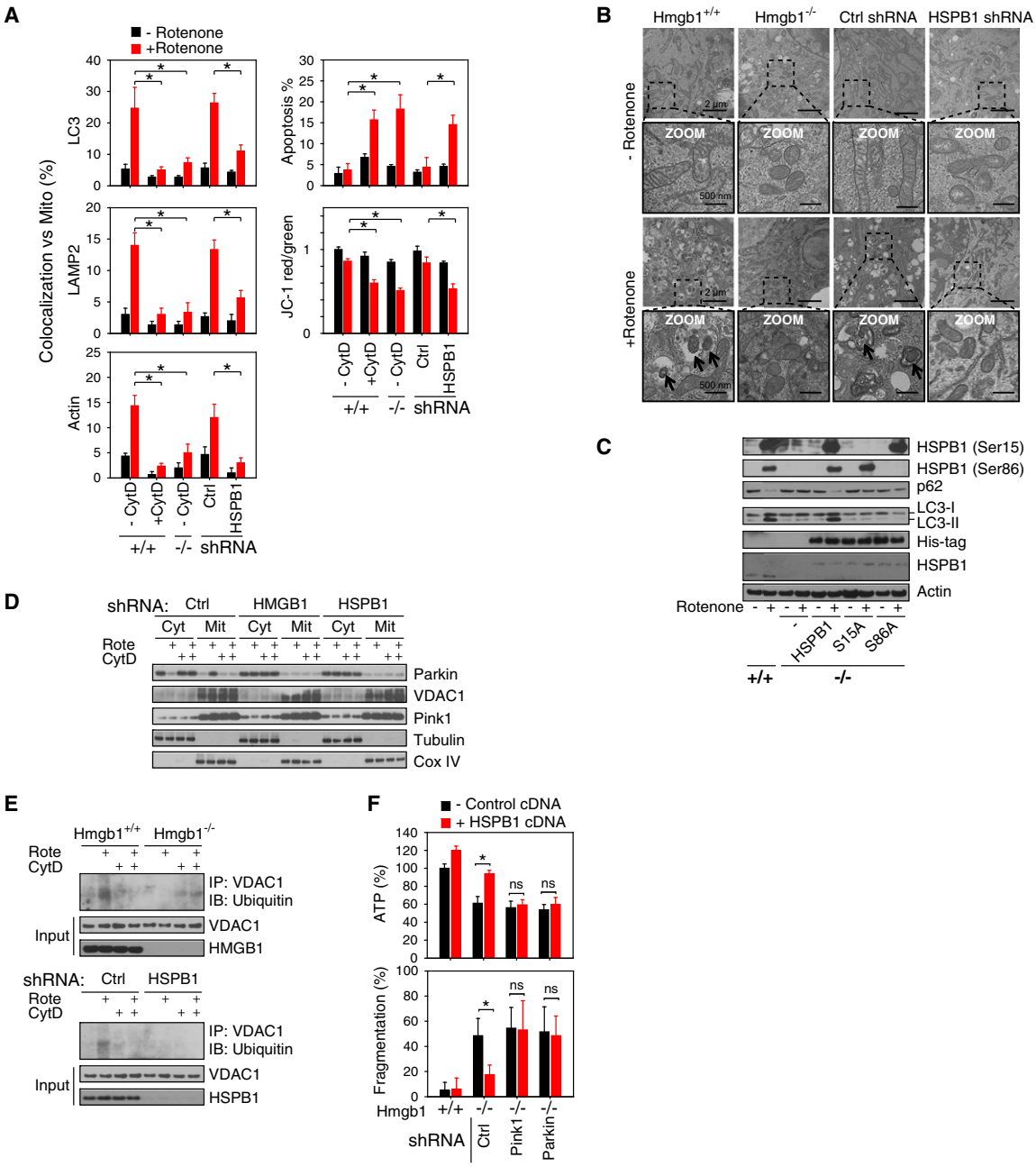

Figure 6. HMGB1 and HSPB1 Regulate Mitophagy after Rotenone-Induced Disruption of Oxidative Phosphorylation

(A) Confocal microscopy colocalizes mitochondria with LC3, LAMP2, and actin in Hmgb1$^{+/+}$ (+/+), Hmgb1$^{-/-}$ (−/−), control shRNA, or HSPB1 shRNA MEFs with or without rotenone (2 uM, 6 hr). Cytochalasin D (CytD, 1 uM, 6 hr) was used to inhibit actin polymerization. Images were acquired digitally from a randomly selected pool of 10–15 fields under each condition. Quantitative analysis of colocalization (%) was performed. Representative images are shown in Figure S4. In parallel, apoptosis was analyzed by the Annexin V-FITC apoptosis detection kit and mitochondrial membrane potential depolarization (the Hmgb1$^{+/+}$ control group was set as 1) was measured by JC-1 fluorescence. Data are expressed as mean ± SD (*$p < 0.01$, n = 3).

(B) Ultrastructural features assessed by electron microscopy in Hmgb1$^{+/+}$, Hmgb1$^{-/-}$, control shRNA, and HSPB1 shRNA MEFs with or without ATP depletion by rotenone (2 uM, 4 hr). Arrows point to mitochondria in autophagosomes or autolysosomes which are not apparent in Hmgb1$^{-/-}$ or HSPB1 knockdowns. The boxed areas represent expanded regions (magnified) from the panels of the selected region by confocal imaging.

(C) ATP depletion by rotenone (2 uM, 6 hr) increased the expression of p-HSPB1 (Ser15 and Ser86) in Hmgb1$^{+/+}$ (+/+) cells but not Hmgb1$^{-/-}$ (−/−) cells. HSPB1 mutants (S15A, S86A) cannot restore the decreased LC3-II and increased p62 expression observed in Hmgb1$^{-/-}$ cells after rotenone treatment.

(D) Cells as indicated were treated with rotenone (2 uM) for 6 hr and then cytoplasmic (Cyt) and mitochondrial (Mit) extracts from cells were separated by SDS-PAGE. The blots were probed with antibody against Parkin, Cox IV, tubulin, VDAC1, and Pink1.

(E) Cells as indicated were treated with rotenone (2 uM) for 6 hr and then VDAC1 ubiquitylation was assayed by immunoprecipitation (IP) and western blot (IB).

(F) Cellular ATP levels and mitochondrial fragmentation was assayed in Hmgb1$^{+/+}$ (+/+) and Hmgb1$^{-/-}$ (−/−) cells transfected with HSPB1 vectors with or without Pink1 or Parkin shRNA (mean ± SD, *$p < 0.01$, ns, not significant).

(Figure 6A). In contrast, expression of HSPB1 in HMGB1-deficient cells undergoing mitochondrial injury restored the interaction between mitochondria and the cytoskeleton and increased the dynamic stages of autophagy (Figure S6).

In response to stress, phosphorylation and increased expression of HSPB1 modulates actin polymerization and reorganization (Lavoie et al., 1993b; Rousseau et al., 1997). We next explored whether alterations in the phosphorylation of HSPB1 (Ser15 and Ser86) influence autophagy. ATP depletion induced by rotenone treatment increased the expression of pHSPB1 (both Ser15 and Ser86) in Hmgb1$^{+/+}$ cells but not in Hmgb1$^{-/-}$ cells (Figure 6C). Previous studies have demonstrated that these phosphorylated HSPB1 mutations decreased F-actin stabilization and had no influence on the chaperone activity of HSPB1 (Benndorf et al., 1994; Rogalla et al., 1999). Expression of phosphorylation-deficient mutants of HSPB1 (S15A and S86A), however, did not restore the deficit in autophagy, ATP production, or morphology, whereas wild-type HSPB1 cDNA did (Figure 6C and Figure S6). These findings suggest that both Ser15 and Ser86 are necessary for HSPB1-mediated autophagy.

Upon mitochondrial membrane depolarization, PTEN-induced putative kinase 1 (Pink1), a kinase of the outer mitochondrial membrane, induces Parkin translocation to stressed mitochondria (Geisler et al., 2010; Narendra et al., 2008). Subsequently, Parkin mediates the formation of ubiquitin chains on voltage-dependent anion channel 1 (VDAC1). This leads to the recruitment of the autophagy receptor p62, which in turn, by binding to LC3, directs damaged mitochondria to the autophagosome (Geisler et al., 2010). There has, however, been a contradictory report showing that VDAC1 may not be required for Parkin-mediated mitophagy (Narendra et al., 2010). We found that loss of HMGB1 or HSPB1 inhibited rotenone-induced Parkin translocation, VDAC1 ubiquitylation (Figures 6D and 6E and Figure S7A), but not Parkin expression (Figures 1A, 2A, 3A, and 5A). Moreover, knockdown of Pink1 or Parkin abolish the HSPB1-restored ATP production and reduced mitochondrial fragmentation in Hmgb1$^{-/-}$ cells (Figure 6F). These findings suggest that both Pink1 and Parkin are required for both HSPB1 and HMGB1-mediated mitophagy.

Although mitophagy is a well established mechanism necessary for elimination of dysfunctional mitochondria and regulation of mitochondrial quality in yeast or mammalian cells by mediators such as NIX (Sandoval et al., 2008), autophagy-related gene 32 (Okamoto et al., 2009), OPA1 (Twig et al., 2008), and DRP1 (Twig et al., 2008), it is unclear whether or how mitophagy triggered by dysfunctional mitochondria is regulated by nuclear mediators. Our findings indicate that the nuclear protein HMGB1 modulates mitochondrial respiration and morphology by helping to sustain autophagy in mitochondria maintenance through regulation of HSPB1 gene expression (Figure 7). Phosphorylation of HSPB1 is necessary to regulate the actin cytoskeleton, which affects the dynamics of autophagy in response to mitochondrial injury. Because loss of either HMGB1 or HSPB1 results in autophagy deficiency, increase in the number of impaired mitochondria results in an apparent increase in mitochondrial fragmentation. Moreover, loss of HMGB1 or HSPB1 results in decreased aerobic respiration and subsequent ATP production. Indeed, deletion of HMGB1 (Calogero et al., 1999) or HSPB1 (Garrido, 2002) in mice results in early postembryonic

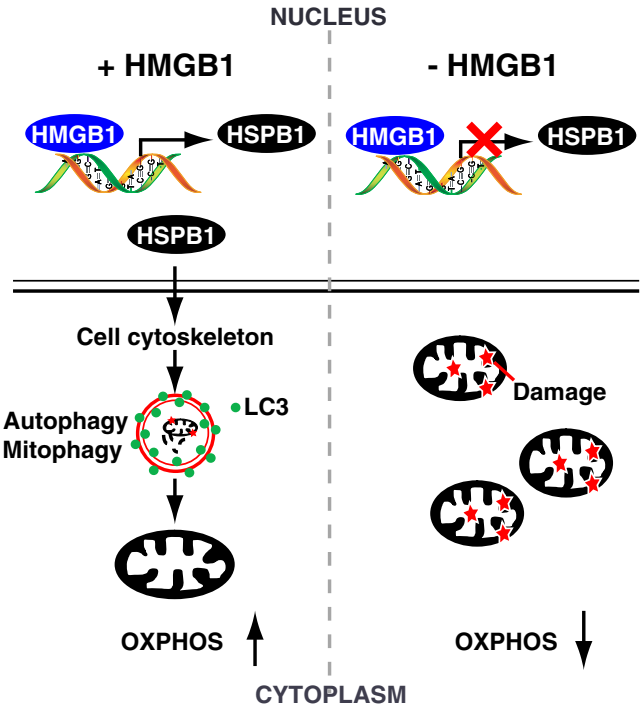

Figure 7. Schematic of the Mechanism by which HMGB1 Modulates Mitochondrial Respiration and Morphology by Sustaining Mitophagy
In wild-type cells, HMGB1 functions as a transcriptional regulator of HSPB1 gene expression. Phosphorylation of HSPB1 is necessary to regulate the actin cytoskeleton, which affects the cellular transport of autophagy and mitophagy in response to mitochondrial injury. Loss of either HMGB1 or HSPB1 results in phenotypically similar deficient mitophagy typified by mitochondrial fragmentation, decreased aerobic respiration, and subsequent ATP production. OXPHOS, oxidative phosphorylation.

lethality. HMGB1 is localized within the nucleus, but in several cell types and environments, HMGB1 can be detected within the cytoplasm and readily within the extracellular space (Lotze and Tracey, 2005). Our recent studies demonstrated that both extracellular (exogenous) and endogenous HMGB1 promote autophagy and cell survival after application of cancer chemotherapeutic agents and nutritional depletion (Liu et al., 2011; Tang et al., 2010a, 2010b). Cytoplasmic HMGB1 is a Beclin 1-binding protein active in autophagy (Kang et al., 2010a; Tang et al., 2010b). Interestingly, rotenone-mediated mitochondrial injury increased the expression of HMGB1 and HSPB1 in mitochondria (Figure S7B), although this change and its significance in the regulation of autophagy and mitophagy is unknown.

The cellular cytoskeleton plays multiple roles in regulation of both selective and nonselective autophagy (Monastyrska et al., 2009). For example, histone deacetylase-6 (HDAC6) promotes autophagy and mitophagy by assembling an F-actin network that stimulates autophagosome-lysosome fusion and substrate degradation (Lee et al., 2010). Interestingly, mitochondria degradation in yeast involves both a selective and nonselective process of autophagy (Kissová et al., 2007). Indeed, some specific regulators of mitophagy also play roles in nonselective autophagy. For example, Parkin-mediated K63-linked polyubiquitination is required for autophagic clearance of misfolded

proteins (Olzmann and Chin, 2008). Nix is important for ROS-mediated autophagy induction (Ding et al., 2010). More recently, the mammalian Atg1 homolog UNC-51-like kinase 1 (ULK1) has been shown to be required for both autophagy and mitophagy after starvation (Egan et al., 2011). Our findings suggest that HMGB1 and HSPB1 coordinately regulate both macroautophagy and mitophagy after starvation and mitochondrial injury. However, it is still unclear as to the actual mechanisms by which selective and nonselective autophagy are regulated. Delineation of discrete autophagic pathways will improve our understanding of both mitophagy and autophagy and will also enable development of therapeutic strategies to target diseases such as Parkinson's disease and cancer.

EXPERIMENTAL PROCEDURES

Reagents

The antibodies to HSP90, HSP70, HSP60, HSP40, HSF1, GFP, B cell leukemia and lymphoma 2 (Bcl-2), and His-tag were obtained from Cell Signaling Technology (Danvers, MA). The antibody to HSP110 was obtained from Stressgen (Ann Arbor, MI). The antibodies to actin, Nix, and HSPB1 (HSP25/27) were obtained from Sigma (St. Louis, MO). The antibodies to pHSPB1 (Ser15), pHSPB1 (Ser86), Pink1, Parkin, VDAC1, and ubiquitin were obtained from Abcam (Cambridge, MA). The antibodies to HMGB1, microtubule-associated proteins LC3-I and LC3-II, DRP1, MEN1, OPA1, and LAMP2 were obtained from Novus (Littleton, CO). The antibodies to αB-crystallin, p62, and FIS1were from Santa Cruz Technology (Santa Cruz, CA,). The antibodies to the complex I subunits NDUFA9 and GRIM-19, complex II subunit 70 kDa Fp, complex III subunit Core 2, complex IV subunit 1, complex V subunit α, cytchrome C, ATP synthase β, and mitofilin were obtained from Mitosciences (Eugene, OR). Hoechst 33342 and phalloidin were obtained from Invitrogen (San Diego, California). All other chemical reagents were obtained from Sigma (St. Louis, MO).

pEGFPN1-HMGB1 plasmid was a kind gift from Dr. George Hoppe (Cole Eye Institute) (Hoppe et al., 2006). The pUNO1-HMGB1 plasmid was obtained from InvivoGen. The pcDNA4-HisMaxC-HSPB1, pcDNA4-HisMaxC-S15A, and pcDNA4-HisMaxC-S86A were kind gifts from Dr. Yoon-Jin Lee (Korea Institute of Radiological and Medical Sciences)(Lee et al., 2005). pEGFPC1-p62 plasmid was a kind gift from Dr. Eileen White (The Cancer Institute of New Jersey) (Mathew et al., 2009). Mouse or human HSPB1 shRNA, HMGB1 shRNA, Pink1 shRNA, and Parkin shRNA were obtained from Sigma. A nuclear and cytoplasmic extraction kit and a mitochondria and membrane isolation kit were obtained from Pierce (Rockford, IL).

Cell Culture

NIH-3T3 fibroblasts, Panc02, Panc2.03, and HCT116 cells were derived from the American Type Culture Collection (Manassas, VA) or National Institutes of Health (Bethesda, MD). Hmgb1$^{+/+}$ and Hmgb1$^{-/-}$ immortalized mouse embryonic fibroblasts were a kind gift from Dr. Marco E. Bianchi (San Raffaele Institute, Italy) (Calogero et al., 1999). All cell lines were cultured in medium supplemented with 10% heat-inactivated fetal bovine serum, 2 mM glutamine and penicillin-streptomycin mix (Invitrogen, final concentration 50 μg/ml each) in a humidified incubator with 5% CO_2 and 95% air.

Gene Transfection and RNAi

Expression vector transfection or shRNA transfection by using FuGENE® HD Transfection Reagent (Roche Applied Science, Stockholm, Sweden) or Lipofectamine 2000 reagent (Life Technologies) were performed according to the manufacturer's instructions. siRNA was transfected into cells by using X-tremeGENE siRNA reagent (Roche Applied Science) according to the manufacturer's instructions. In general, the transfection efficiency is >80%.

Western Blotting

Proteins in cell lysates were resolved on 4%–12% Criterion XT Bis-Tris gels (Bio-Rad) and transferred to a nitrocellulose membrane as previously described (Tang et al., 2007a, 2007b). After blocking, the membrane was incubated overnight at 4°C with various primary antibodies. After incubation with peroxidase-conjugated secondary antibodies for 1 hr at 25°C, signals were visualized by enhanced chemiluminescence detection (Pierce) according to the manufacturer's instruction. The relative band intensities were quantified by using the Gel-Pro Analyzer® software (Media Cybernetics, Bethesda, MD).

Immunofluorescence Analysis

Cells were cultured on glass coverslips and fixed in 3% formaldehyde for 30 min at room temperature prior to detergent extraction with 0.1% Triton X-100 for 10 min at 25°C. Coverslips were saturated with 2% bovine serum albumin (BSA) in phosphate-buffered saline (PBS) for 1 hr at room temperature and processed for immunofluorescence with primary antibodies followed by Alexa Fluor or Cy3-conjugated secondary antibodies, respectively. Nuclear morphology was analyzed with the fluorescent dye Hoechst 33342. Actin was stained with phalloidin. Mitochondria were stained by using anti-complex I subunit GRIM-19 or anti-ATP synthase β. Between all incubation steps, cells were washed three times for 3 min with 0.5% BSA in PBS. Images were taken with an Olympus Fluoview 1000 confocal microscope (Olympus Corp., Tokyo, Japan). Fluorescent intensities were measured by Image-Pro Plus platform (Media Cybernetics, Bethesda, MD). The mitochondria of untreated cells were filamentous and showed a thread-like tubular structure, while mitochondria in stressed cells were fragmented and appeared shortened and punctate. Quantification of mitochondrial fragmentation was performed as described previously (Brooks et al., 2009).

Immunoprecipitation Analysis

Cells were lysed at 4°C in ice-cold modified radioimmunoprecipitation lysis buffer (Millipore, Billerica, MA) and cell lysates were cleared by centrifugation at 12000 *g* for 10 min. Concentrations of proteins in the supernatant were determined by bicinchoninic acid assay. Prior to immunoprecipitation, samples containing equal amount of proteins were precleared with protein A or protein G agarose or sepharose (Millipore) (4°C, 3 hr) and subsequently incubated with various irrelevant IgG or specific antibodies (2–5 μg/ml) in the presence of protein A or G agarose or sepharose beads for 2 hr or overnight at 4°C with gentle shaking. After incubation, agarose or sepharose beads were washed extensively with PBS and proteins were eluted by boiling in 2 × sodium dodecyl sulfate (SDS) sample buffer before SDS-PAGE electrophoresis. To detect ubiquitylation of VDAC1, we immunoprecipitated cell extracts with anti-VDAC1 antibody and analyzed them with an anti-ubiquitin antibody followed by western blotting.

ATP Assay

The ATP content in whole-cell extracts was determined with a luminescent ATP detection kit (ATPlite, PerkinElmer, Boston, MA) according to the manufacturer's instructions. The luminescent intensity was measured by using a microplate reader (Synergy 2, BioTek Instruments, Winooski, VT). In parallel, the cell numbers in whole-cell samples were counted by trypan blue exclusion assay. The results were expressed as relative ATP level compared with controls after normalizing for cell numbers.

Autophagy Assays

The percentage of cells with LC3 punctae was determined by quantifying the number of positively staining cells from 50–100 randomly chosen cells from 15–20 random fields. Autophagic flux assays were performed by western blotting for LC3-I and LC3-II and p62, by imaging for the percentage of cells with LC3 and p62 punctae, and by colocalization of LC3 with mitochondria, actin with mitochondria, and LAMP2 with mitochondria. In brief, images were collected by using a laser scanning confocal microscope (Fluoview FV-1000, Olympus) with a 60 × Plan Apo 1.45 oil immersion objective at 25°C and Fluoview software (FV10-ASW 1.6, Olympus). Images were subsequently analyzed for fluorescent intensity levels and colocalization of various stains by Image-Pro Plus 5.1 software (Media Cybernetics).

Transmission electron microscopic (TEM) assessment of autophagosomes and autolysosomes was performed as previously described (Tang et al., 2010b). In brief, cells were fixed with 2% paraformaldehyde and 2% glutaraldehyde in 0.1 mol/L phosphate buffer (pH 7.4), followed by incubation for 6 hr in 1% O_sO_4. After dehydration with graded alcohols, the samples were embedded in epoxy resin (Epon, Momentive Specialty Chemicals, Houston,

TX). After embedding, thin sections (70 nm) were cut by using a microtome (Leica Ultracut R), mounted on copper grids and poststained with 2% uranyl acetate and 1% lead citrate, dried, and analyzed by using a TEM at 25°C (JEOL 100CX, Peabody, MA). Thick sections were cut (300 nm) and stained with 1% toluidine blue. Images were acquired digitally from a randomly selected pool of 10–15 fields under each condition.

Apoptosis Assays

Apoptosis in cells was assessed with the Annexin V-FITC Apoptosis Detection Kit (BD PharMingen, San Jose, CA) by using flow cytometric analysis (Kang et al., 2010c; Tang et al., 2010a) or a TUNEL kit from Roche Applied Science. Mitochondrial membrane potential depolarization was measured by flow cytometry with a fluorescent cationic dye, 1,1′3,3′- tetraethylbenzamidazolocarbocyanin iodide (JC-1, Molecular Probes, San Diego, CA). JC-1 dye exhibits potential-dependent accumulation in mitochondria, indicated by a fluorescence emission shift from green (~529 nm) to red (~590 nm). Consequently, mitochondrial depolarization is assessed by a decrease in the red/green fluorescence intensity ratio.

Heat Shock Element Activation Assay

Cells were transiently transfected in a 12-well plate with an HSE luciferase reporter plasmid and control empty plasmid by using Lipofectamine 2000 reagent (Invitrogen) according to the manufacturer's instructions. After 24–48 hr, the cells were exposed to various treatments. Luciferase activity was determined by using an assay system including the reporter lysis buffer obtained from Promega (Madison, WI) as described previously (Wang et al., 2002). The results were expressed as relative HSE activity after normalizing for the control empty plasmid.

Oxidative Phosphorylation and Glycolysis Assay

Cellular OXPHOS and glycolysis were monitored with the Seahorse Bioscience Extracellular Flux Analyzer (XF24, Seahorse Bioscience Inc., North Billerica, MA) by measuring the OCR (indicative of respiration) and ECR (indicative of glycolysis) in real time as previously described (Qian and Van Houten, 2010; Wu et al., 2007). Briefly, 30,000–50,000 cells were seeded in 24-well plates designed for XF24 in 150 μl of appropriate growth media and incubated overnight. Prior to measurements, cells were washed with unbuffered media once, then immersed in 675 μl unbuffered media and incubated in the absence of CO_2 for 1 hr. The OCR and ECR were then measured in a typical 8 min cycle of mix (2–4 min), dwell (2 min) and measure (2–4 min) as recommended by Seahorse Bioscience. The basal levels of OCR and ECR were recorded first, followed by the OCR and ECR levels after injection of compounds that inhibit the respiratory mitochondrial electron transport chain, ATP synthesis, or glycolysis.

Subcellular Fractionation and Organelle Isolation

Subcellular fractionation of cells was carried out according to the manufacturer's instructions with a mitochondria, membrane, or nuclear isolation kit obtained from Pierce (Rockford, IL).

Statistical Analysis

Data are expressed as means ± SD of two or three independent experiments performed in triplicate. One-way ANOVA was used for comparison among the different groups. When the ANOVA was significant, post hoc testing of differences between groups was performed by using an LSD test. A p value < 0.05 was considered significant.

SUPPLEMENTAL INFORMATION

Supplemental Information includes seven figures and can be found with this article online at doi:10.1016/j.cmet.2011.04.008.

ACKNOWLEDGMENTS

This project was funded by 1PO1CA101944 from the National Institutes of Health (M.T.L.), start-up funding from the University of Pittsburgh (D.T.) and Pennsylvania Commonwealth Universal Research Enhancement Program (B.V.H.). We thank Dr. George Hoppe (Cole Eye Institute) for pEGFPN1-HMGB1; Dr. Yoon-Jin Lee (Korea Institute of Radiological and Medical Sciences) for pcDNA4-HisMaxC-HSPB1, pcDNA4-HisMaxC-S15A, and pcDNA4-HisMaxC-S86A; Dr. Marco E. Bianchi (San Raffaele Institute, Milan, Italy) for $Hmgb1^{+/+}$ and $Hmgb1^{-/-}$ MEFs; Dr. Eileen White (The Cancer Institute of New Jersey) for pEGFPC1-p62; and Drs. Patricia Loughran, Donna B. Stolz, and Simon Watkins (Center for Biologic Imaging, University of Pittsburgh Medical Center) for EM sample preparation and image analysis. Expert technical assistance from Nicole Schapiro and William Buchser, Ph.D., is appreciated.

Received: September 26, 2010
Revised: January 10, 2011
Accepted: April 1, 2011
Published: June 7, 2011

REFERENCES

Arrigo, A.P. (2007). The cellular "networking" of mammalian Hsp27 and its functions in the control of protein folding, redox state and apoptosis. Adv. Exp. Med. Biol. *594*, 14–26.

Benndorf, R., Hayess, K., Ryazantsev, S., Wieske, M., Behlke, J., and Lutsch, G. (1994). Phosphorylation and supramolecular organization of murine small heat shock protein HSP25 abolish its actin polymerization-inhibiting activity. J. Biol. Chem. *269*, 20780–20784.

Bjørkøy, G., Lamark, T., Brech, A., Outzen, H., Perander, M., Overvatn, A., Stenmark, H., and Johansen, T. (2005). p62/SQSTM1 forms protein aggregates degraded by autophagy and has a protective effect on huntingtin-induced cell death. J. Cell Biol. *171*, 603–614.

Boldogh, I.R., and Pon, L.A. (2006). Interactions of mitochondria with the actin cytoskeleton. Biochim. Biophys. Acta *1763*, 450–462.

Brooks, C., Wei, Q., Cho, S.G., and Dong, Z. (2009). Regulation of mitochondrial dynamics in acute kidney injury in cell culture and rodent models. J. Clin. Invest. *119*, 1275–1285.

Calogero, S., Grassi, F., Aguzzi, A., Voigtländer, T., Ferrier, P., Ferrari, S., and Bianchi, M.E. (1999). The lack of chromosomal protein Hmg1 does not disrupt cell growth but causes lethal hypoglycaemia in newborn mice. Nat. Genet. *22*, 276–280.

Chan, D.C. (2006a). Mitochondria: dynamic organelles in disease, aging, and development. Cell *125*, 1241–1252.

Chan, D.C. (2006b). Mitochondrial fusion and fission in mammals. Annu. Rev. Cell Dev. Biol. *22*, 79–99.

Chen, Y., McMillan-Ward, E., Kong, J., Israels, S.J., and Gibson, S.B. (2007). Mitochondrial electron-transport-chain inhibitors of complexes I and II induce autophagic cell death mediated by reactive oxygen species. J. Cell Sci. *120*, 4155–4166.

Clark, I.E., Dodson, M.W., Jiang, C., Cao, J.H., Huh, J.R., Seol, J.H., Yoo, S.J., Hay, B.A., and Guo, M. (2006). Drosophila pink1 is required for mitochondrial function and interacts genetically with parkin. Nature *441*, 1162–1166.

Craig, E.A., Weissman, J.S., and Horwich, A.L. (1994). Heat shock proteins and molecular chaperones: mediators of protein conformation and turnover in the cell. Cell *78*, 365–372.

Ding, W.X., Ni, H.M., Li, M., Liao, Y., Chen, X., Stolz, D.B., Dorn, G.W., 2nd, and Yin, X.M. (2010). Nix is critical to two distinct phases of mitophagy, reactive oxygen species-mediated autophagy induction and Parkin-ubiquitin-p62-mediated mitochondrial priming. J. Biol. Chem. *285*, 27879–27890.

Egan, D.F., Shackelford, D.B., Mihaylova, M.M., Gelino, S.R., Kohnz, R.A., Mair, W., Vasquez, D.S., Joshi, A., Gwinn, D.M., Taylor, R., et al. (2011). Phosphorylation of ULK1 (hATG1) by AMP-activated protein kinase connects energy sensing to mitophagy. Science *331*, 456–461.

Garrido, C. (2002). Size matters: of the small HSP27 and its large oligomers. Cell Death Differ. *9*, 483–485.

Geisler, S., Holmström, K.M., Skujat, D., Fiesel, F.C., Rothfuss, O.C., Kahle, P.J., and Springer, W. (2010). PINK1/Parkin-mediated mitophagy is dependent on VDAC1 and p62/SQSTM1. Nat. Cell Biol. *12*, 119–131.

Hoppe, G., Talcott, K.E., Bhattacharya, S.K., Crabb, J.W., and Sears, J.E. (2006). Molecular basis for the redox control of nuclear transport of the structural chromatin protein Hmgb1. Exp. Cell Res. *312*, 3526–3538.

Kang, R., Livesey, K.M., Zeh, H.J., Loze, M.T., and Tang, D. (2010a). HMGB1: a novel Beclin 1-binding protein active in autophagy. Autophagy *6*, 1209–1211.

Kang, R., Tang, D., Schapiro, N.E., Livesey, K.M., Farkas, A., Loughran, P., Bierhaus, A., Lotze, M.T., and Zeh, H.J. (2010b). The receptor for advanced glycation end products (RAGE) sustains autophagy and limits apoptosis, promoting pancreatic tumor cell survival. Cell Death Differ. *17*, 666–676.

Kang, R., Tang, D., Yu, Y., Wang, Z., Hu, T., Wang, H., and Cao, L. (2010c). WAVE1 regulates Bcl-2 localization and phosphorylation in leukemia cells. Leukemia *24*, 177–186.

Kim, I., Rodriguez-Enriquez, S., and Lemasters, J.J. (2007). Selective degradation of mitochondria by mitophagy. Arch. Biochem. Biophys. *462*, 245–253.

Kissová, I., Salin, B., Schaeffer, J., Bhatia, S., Manon, S., and Camougrand, N. (2007). Selective and non-selective autophagic degradation of mitochondria in yeast. Autophagy *3*, 329–336.

Kroemer, G., Mariño, G., and Levine, B. (2010). Autophagy and the integrated stress response. Mol. Cell *40*, 280–293.

Lavoie, J.N., Gingras-Breton, G., Tanguay, R.M., and Landry, J. (1993a). Induction of Chinese hamster HSP27 gene expression in mouse cells confers resistance to heat shock. HSP27 stabilization of the microfilament organization. J. Biol. Chem. *268*, 3420–3429.

Lavoie, J.N., Hickey, E., Weber, L.A., and Landry, J. (1993b). Modulation of actin microfilament dynamics and fluid phase pinocytosis by phosphorylation of heat shock protein 27. J. Biol. Chem. *268*, 24210–24214.

Lee, Y.J., Lee, D.H., Cho, C.K., Bae, S., Jhon, G.J., Lee, S.J., Soh, J.W., and Lee, Y.S. (2005). HSP25 inhibits protein kinase C delta-mediated cell death through direct interaction. J. Biol. Chem. *280*, 18108–18119.

Lee, J.Y., Koga, H., Kawaguchi, Y., Tang, W., Wong, E., Gao, Y.S., Pandey, U.B., Kaushik, S., Tresse, E., Lu, J., et al. (2010). HDAC6 controls autophagosome maturation essential for ubiquitin-selective quality-control autophagy. EMBO J. *29*, 969–980.

Liu, L., Yang, M., Kang, R., Wang, Z., Zhao, Y., Yu, Y., Xie, M., Yin, X., Livesey, K.M., Lotze, M.T., et al. (2011). HMGB1-induced autophagy promotes chemotherapy resistance in leukemia cells. Leukemia *25*, 23–31.

Lotze, M.T., and Tracey, K.J. (2005). High-mobility group box 1 protein (HMGB1): nuclear weapon in the immune arsenal. Nat. Rev. Immunol. *5*, 331–342.

Mathew, R., Karp, C.M., Beaudoin, B., Vuong, N., Chen, G., Chen, H.Y., Bray, K., Reddy, A., Bhanot, G., Gelinas, C., et al. (2009). Autophagy suppresses tumorigenesis through elimination of p62. Cell *137*, 1062–1075.

Mizushima, N., and Yoshimori, T. (2007). How to interpret LC3 immunoblotting. Autophagy *3*, 542–545.

Monastyrska, I., Rieter, E., Klionsky, D.J., and Reggiori, F. (2009). Multiple roles of the cytoskeleton in autophagy. Biol. Rev. Camb. Philos. Soc. *84*, 431–448.

Moon, Y., Lee, K.H., Park, J.H., Geum, D., and Kim, K. (2005). Mitochondrial membrane depolarization and the selective death of dopaminergic neurons by rotenone: protective effect of coenzyme Q10. J. Neurochem. *93*, 1199–1208.

Narendra, D., Tanaka, A., Suen, D.F., and Youle, R.J. (2008). Parkin is recruited selectively to impaired mitochondria and promotes their autophagy. J. Cell Biol. *183*, 795–803.

Narendra, D., Kane, L.A., Hauser, D.N., Fearnley, I.M., and Youle, R.J. (2010). p62/SQSTM1 is required for Parkin-induced mitochondrial clustering but not mitophagy; VDAC1 is dispensable for both. Autophagy *6*, 1090–1106.

Okamoto, K., Kondo-Okamoto, N., and Ohsumi, Y. (2009). Mitochondria-anchored receptor Atg32 mediates degradation of mitochondria via selective autophagy. Dev. Cell *17*, 87–97.

Olzmann, J.A., and Chin, L.S. (2008). Parkin-mediated K63-linked polyubiquitination: a signal for targeting misfolded proteins to the aggresome-autophagy pathway. Autophagy *4*, 85–87.

Poyton, R.O., and McEwen, J.E. (1996). Crosstalk between nuclear and mitochondrial genomes. Annu. Rev. Biochem. *65*, 563–607.

Qi, M.L., Tagawa, K., Enokido, Y., Yoshimura, N., Wada, Y., Watase, K., Ishiura, S., Kanazawa, I., Botas, J., Saitoe, M., et al. (2007). Proteome analysis of soluble nuclear proteins reveals that HMGB1/2 suppress genotoxic stress in polyglutamine diseases. Nat. Cell Biol. *9*, 402–414.

Qian, W., and Van Houten, B. (2010). Alterations in bioenergetics due to changes in mitochondrial DNA copy number. Methods *51*, 452–457.

Rogalla, T., Ehrnsperger, M., Preville, X., Kotlyarov, A., Lutsch, G., Ducasse, C., Paul, C., Wieske, M., Arrigo, A.P., Buchner, J., and Gaestel, M. (1999). Regulation of Hsp27 oligomerization, chaperone function, and protective activity against oxidative stress/tumor necrosis factor alpha by phosphorylation. J. Biol. Chem. *274*, 18947–18956.

Rousseau, S., Houle, F., Landry, J., and Huot, J. (1997). p38 MAP kinase activation by vascular endothelial growth factor mediates actin reorganization and cell migration in human endothelial cells. Oncogene *15*, 2169–2177.

Sandoval, H., Thiagarajan, P., Dasgupta, S.K., Schumacher, A., Prchal, J.T., Chen, M., and Wang, J. (2008). Essential role for Nix in autophagic maturation of erythroid cells. Nature *454*, 232–235.

Schweers, R.L., Zhang, J., Randall, M.S., Loyd, M.R., Li, W., Dorsey, F.C., Kundu, M., Opferman, J.T., Cleveland, J.L., Miller, J.L., and Ney, P.A. (2007). NIX is required for programmed mitochondrial clearance during reticulocyte maturation. Proc. Natl. Acad. Sci. USA *104*, 19500–19505.

Sorger, P.K. (1991). Heat shock factor and the heat shock response. Cell *65*, 363–366.

Stroikin, Y., Dalen, H., Lööf, S., and Terman, A. (2004). Inhibition of autophagy with 3-methyladenine results in impaired turnover of lysosomes and accumulation of lipofuscin-like material. Eur. J. Cell Biol. *83*, 583–590.

Suen, D.F., Norris, K.L., and Youle, R.J. (2008). Mitochondrial dynamics and apoptosis. Genes Dev. *22*, 1577–1590.

Tang, D., Kang, R., Xiao, W., Jiang, L., Liu, M., Shi, Y., Wang, K., Wang, H., and Xiao, X. (2007a). Nuclear heat shock protein 72 as a negative regulator of oxidative stress (hydrogen peroxide)-induced HMGB1 cytoplasmic translocation and release. J. Immunol. *178*, 7376–7384.

Tang, D., Shi, Y., Kang, R., Li, T., Xiao, W., Wang, H., and Xiao, X. (2007b). Hydrogen peroxide stimulates macrophages and monocytes to actively release HMGB1. J. Leukoc. Biol. *81*, 741–747.

Tang, D., Kang, R., Cheh, C.W., Livesey, K.M., Liang, X., Schapiro, N.E., Benschop, R., Sparvero, L.J., Amoscato, A.A., Tracey, K.J., et al. (2010a). HMGB1 release and redox regulates autophagy and apoptosis in cancer cells. Oncogene *29*, 5299–5310.

Tang, D., Kang, R., Livesey, K.M., Cheh, C.W., Farkas, A., Loughran, P., Hoppe, G., Bianchi, M.E., Tracey, K.J., Zeh, H.J., 3rd, and Lotze, M.T. (2010b). Endogenous HMGB1 regulates autophagy. J. Cell Biol. *190*, 881–892.

Tang, D., Kang, R., Zeh, H.J., 3rd, and Lotze, M.T. (2010c). High-mobility group box 1 and cancer. Biochim. Biophys. Acta *1799*, 131–140.

Tang, D., Kang, R., Zeh, H.J., 3rd, and Lotze, M.T. (2011). High-mobility group box 1, oxidative stress, and disease. Antioxid. Redox Signal. *14*, 1315–1335.

Tatsuta, T., and Langer, T. (2008). Quality control of mitochondria: protection against neurodegeneration and ageing. EMBO J. *27*, 306–314.

Twig, G., Elorza, A., Molina, A.J., Mohamed, H., Wikstrom, J.D., Walzer, G., Stiles, L., Haigh, S.E., Katz, S., Las, G., et al. (2008). Fission and selective fusion govern mitochondrial segregation and elimination by autophagy. EMBO J. *27*, 433–446.

Wang, S., Kotamraju, S., Konorev, E., Kalivendi, S., Joseph, J., and Kalyanaraman, B. (2002). Activation of nuclear factor-kappaB during doxorubicin-induced apoptosis in endothelial cells and myocytes is pro-apoptotic: the role of hydrogen peroxide. Biochem. J. *367*, 729–740.

Wu, M., Neilson, A., Swift, A.L., Moran, R., Tamagnine, J., Parslow, D., Armistead, S., Lemire, K., Orrell, J., Teich, J., et al. (2007). Multiparameter metabolic analysis reveals a close link between attenuated mitochondrial bioenergetic function and enhanced glycolysis dependency in human tumor cells. Am. J. Physiol. Cell Physiol. *292*, C125–C136.

Yang, Z., and Klionsky, D.J. (2010). Eaten alive: a history of macroautophagy. Nat. Cell Biol. *12*, 814–822.

Youle, R.J., and Narendra, D.P. (2011). Mechanisms of mitophagy. Nat. Rev. Mol. Cell Biol. *12*, 9–14.